Surface Science 604 (2010) 1757–1766

Contents lists available at ScienceDirect

Surface Science

journal homepage: www.elsevier.com/ locate/susc

Structural and electronic properties of group III Rich $In_{0.53}Ga_{0.47}As(001)$

Jian Shen [a,b], Jonathon B. Clemens [b], Evgueni A. Chagarov [b], Darby L. Feldwinn [b], Wilhelm Melitz [a,b], Tao Song [b], Sarah R. Bishop [b], Andrew C. Kummel [b,*], Ravi Droopad [c]

[a] Materials Science & Engineering Program, San Diego, La Jolla, CA 92093, USA
[b] Department of Chemistry and Biochemistry University of California, San Diego, La Jolla, CA 92093, USA
[c] Department of Physics, Texas State University, San Marcos, Texas 78666, USA

ARTICLE INFO

Article history:
Received 4 October 2009
Accepted 2 July 2010
Available online 15 July 2010

Keywords:
Density functional calculations
Scanning tunneling microscopy
Scanning tunneling spectroscopies
Semiconducting surfaces
Surface relaxation and reconstruction
Indium gallium arsenide
Bader charge

ABSTRACT

The structural and electronic properties of group III rich $In_{0.53}Ga_{0.47}As(001)$ have been studied using scanning tunneling microscopy/spectroscopy (STM/STS). At room temperature (300 K), STM images show that the $In_{0.53}Ga_{0.47}As(001)$–(4×2) reconstruction is comprised of undimerized In/Ga atoms in the top layer. Quantitative comparison of the $In_{0.53}Ga_{0.47}As(001)$–(4×2) and InAs(001)–(4×2) shows the reconstructions are almost identical, but $In_{0.53}Ga_{0.47}As(001)$–(4×2) has at least a 4× higher surface defect density even on the best samples. At low temperature (77 K), STM images show that the most probable $In_{0.53}Ga_{0.47}As(001)$ reconstruction is comprised of one In/Ga dimer and two undimerized In/Ga atoms in the top layer in a double (4×2) unit cell. Density functional theory (DFT) simulations at elevated temperature are consistent with the experimentally observed 300 K structure being a thermal superposition of three structures. DFT molecular dynamics (MD) show the row dimer formation and breaking is facilitated by the very large motions of tricoodinated row edge As atoms and z motion of In/Ga row atoms induced changes in As–In/Ga–As bond angles at elevated temperature. STS results show there is a surface dipole or the pinning states near the valence band (VB) for 300 K $In_{0.53}Ga_{0.47}As(001)$–(4×2) surface consistent with DFT calculations. DFT calculations of the band-decomposed charge density indicate that the strained unbuckled trough dimers being responsible for the surface pinning.

1. Introduction

III–V compound semiconductors are becoming increasingly important for a wide range of potential applications such as optoelectronic devices and high-speed, low-power logic applications, owing to their high electron mobilities, direct bandgaps, and high breakdown voltages. Nearly all these devices employ oxide-semiconductor, metal-semiconductor, or semiconductor–semiconductor interfaces. Therefore, it is necessary to understand the chemistry and physics of III–V compound semiconductors' atomic-scale surface reconstructions since they play a critical role in interface formation.

$In_{0.53}Ga_{0.47}As$ is a convenient III–V compound semiconductor for a metal–oxide–semiconductor field-effect transistor (MOSFET) channel material due to its high electronic mobility (~14,000 $cm^2\ V^{-1}\ s^{-1}$), high breakdown field, and its ability to be grown lattice matched on the semi-insulator substrate, InP. The key to fabricating a practical III–V MOSFET is forming an unpinned oxide–semiconductor interface with low fixed charge and low trap density. The interface quality between the oxide and III–V compound semiconductor has been found to correlate with the type of semiconductor surface reconstruction [1]. Although the As-rich InGaAs(001)–(2×4) and (4×3) reconstructions have been the focus of many scanning tunneling microscopy (STM) investigations and a few theoretical studies [2–4], there is still no consensus on the surface structure of the group III rich $In_{0.53}Ga_{0.47}As$ (001)–(4×2). The group III rich reconstructions may be especially important for gate oxides deposition. It is likely that the As-rich (2×4) reconstruction undergoes oxygen induced displacement reactions during gate oxide deposition because the dimerized arsenic atoms are likely to be displaced by ambient oxygen during oxide deposition [5–8]. Conversely, the group III rich (4×2) reconstructions are less reactive to oxygen and, therefore, probably more suitable for oxide deposition [9].

In this report, the first study of the surface reconstructions of the group III rich $In_{0.53}Ga_{0.47}As(001)$ at both 300 K room temperature (RT) and 77 K low temperature (LT), using STM is presented. STM images of the $In_{0.53}Ga_{0.47}As(001)$ show that the surface structures are different at 300 K and 77 K. At 300 K, the $In_{0.53}Ga_{0.47}As(001)$–(4×2) surface appears to have only undimerized group III In/Ga topmost row atoms. At 77 K, the $In_{0.53}Ga_{0.47}As(001)$–(4×2) surface has both undimerized and dimerized group III In/Ga topmost row atoms. The RT and LT reconstructions observed by STM for $In_{0.53}Ga_{0.47}As(001)$–(4×2) are nearly identical to those observed by STM for InAs(001)–(4×2). Standard DFT shows a bandgap for InGaAs(001) in contrast to InAs(001); therefore, the modeling of InGaAs(001) allows reasonably accurate calculations of the electronic structure for comparison to

* Corresponding author.
E-mail addresses: jimshen@ucsd.edu (J. Shen), akummel@ucsd.edu (A.C. Kummel).

0039-6028/$ – see front matter © 2010 Elsevier B.V. All rights reserved.
doi:10.1016/j.susc.2010.07.001

experimental results. For both $In_{0.53}Ga_{0.47}As(001)$–(4×2) and InAs (001)–(4×2) density functional theory (DFT) simulations predict that undimerized and dimerized structures have an energy difference of less than 10 meV per surface atom consistent with the 300 K structure not being a completely different structure than the 77 K structure but instead being a thermal superposition of three nearly degenerate structures; this was confirmed using DFT molecular dynamics (MD) simulations at elevated temperature. Both scanning tunneling spectroscopy (STS) and DFT calculations show that the $In_{0.53}Ga_{0.47}As(001)$–(4×2) 300 K structure is pinned.

2. Experimental and theoretical methods

MBE was employed to grow a 0.2 μm layer of 1×10^{18} cm^{-3} doped $In_{0.53}Ga_{0.47}As$, lattice matched on 500 μm thick InP(001) substrates (Wafer Technology) with 1×10^{18} cm^{-3} doping. Experiments were performed on both n-type and p-type wafers. The re-grown wafers were capped in situ with a 50 nm protective As_2 cap. The wafers were transferred to a vacuum container for transporting to the STM chamber. The STM chamber is equipped with low energy electron diffraction (LEED) for determination of the surface periodicity. Omicron VT-STM and LT-STM spectrometers were employed for determination of atomic structure at 300 K and 77 K. All the experiments were performed in ultra-high vacuum (UHV) systems with a background pressure less than 8×10^{-11} Torr. The As_2 capped samples were radiatively heated to obtain the desired $In_{0.53}Ga_{0.47}As(001)$ surface reconstruction. A three step decapping and annealing procedure was performed. First, the samples were initially held at 180 °C for at least 2 h of degassing. This removed the weakly bonded impurities from the surface such as water. Second, the sample temperature was raised to 330 °C for typically between 2 and 4 h to remove the As-cap. Finally, the sample was gradually heated to the peak temperature (around 450 °C for InAs (001)–(4×2) and 460 °C for $In_{0.53}Ga_{0.47}As(001)$–(4×2)) and held for 15 min followed by a quick quenching. Following the As-decapping and annealing procedure, the surface reconstruction was verified by LEED. Afterwards, the sample was transferred into the STM chamber. STM images were taken at both 300 K room temperature and 77 K low temperature. Typical imaging conditions for both room temperature and low temperature are constant-current mode with a typical 50–100 pA setpoint tunneling current and −2 V sample bias voltage relative to the tungsten tip.

All DFT simulations were performed with the Vienna Ab-initio Simulation Package (VASP) [10,11] using projector augmented-wave (PAW) pseudopotentials (PP) [12,13] and PBE (Perdew-Burke-Ernzerhof) exchange-correlation functional [14,15]. The choice of PBE functional and PAW PP's was validated by parametrization runs demonstrating good reproducibility of experimental lattice constants, bulk moduli, and formation energies for bulk crystalline GaAs, and InAs. A Brillouin zone integration was performed at 4×4×1 Monkhorst–Pack k-point mesh with 9 irreducible k-points and a plane wave energy cut-off of 250 eV. A double (4×2) reconstructed unit cell (~16.95×16.95 $Å^2$, 140 atoms) was used, consisting of 7 atomic layers with a (001) surface orientation. The bottom layer As atoms were passivated by H atoms with fractional 3/4 |e| charge to mimic a continuous InGaAs bulk according to Ref. [16]. The slabs were relaxed using Conjugate-Gradient (CG) relaxation algorithms with 0.05 eV/Å force tolerance level. During relaxation, the three bottom layers were fixed in their bulk positions. A vacuum layer of ~12 Å was added over the slabs to eliminate spurious interaction through periodic boundary conditions (PBC). To compensate for spurious electric field induced by PBC for this type of system, a dipole correction was applied [10,11,17]. The preliminary $In_{0.5}Ga_{0.5}As$ bulk unit cell was formed from GaAs unit cell by substituting half of Ga atoms by In atoms following checkerboard pattern and DFT optimizing the lattice constant of the alloy to equilibrium value. All slab total energies are reported per double (4×2) unit cell.

3. Results and discussions

3.1. Experimental results

3.1.1. Room temperature 300 K $In_{0.53}Ga_{0.47}As$ Surface

Shown in Fig. 1a is a typical large scale filled state RT-STM image of $In_{0.53}Ga_{0.47}As(001)$ surface after As-decapping and annealing at 460 °C. The surface exhibits large, well-ordered, flat terraces. The main feature for the group III rich $In_{0.53}Ga_{0.47}As(001)$ surface is rows running in the [110] direction. The distance between the rows is 17 Å. Between the rows are trough regions. STM images reveal that this (4×2) surface is similar to the surface reconstructions of several other low bandgap III–V materials like InSb(001)–(4×2) and InAs(001)–(4×2) surfaces, which have been observed by several groups [18–23]. However it is distinct from the Ga-rich GaAs(001)–(4×2) reconstruction [24–29]. Detailed reports of the surface reconstructions on GaAs(001) can been found in reports by Northrup et al. and Chadi et al. [24,30–33].

A quantitative comparison of the surface defect density on InAs (001)–(4×2) and $In_{0.53}Ga_{0.47}As(001)$–(4×2) was performed. Filled state STM images of group III rich InAs(001)–(4×2) and $In_{0.53}Ga_{0.47}As$ (001)–(4×2) surface are shown in Fig. 1a and b for comparison. The absence of chemical impurities on the surface was confirmed by X-ray photoelectron spectroscopy (XPS): no C and O peaks were found on the clean surface. For both clean (4×2) surfaces, there are at least four kinds of defects on the both surfaces. Fig. 1a shows the following defects types (D_n): D_1 as dark cuts on the row, D_2 as protrusion dots between the rows, D_3 domain boundaries as depression lines in the [−110] direction and D_4 domain boundaries as protrusion lines in the [110] direction. It is difficult to compare D_2, D_3 and D_4 defects between InAs and $In_{0.53}Ga_{0.47}As$ clean surfaces because quantities of these three defects are small or almost zero on the InAs(001)–(4×2) clean surface, so statistical errors are likely to occur. Therefore, only D_1 defects are analyzed. For the D_1 defects in Fig. 1a, there are 108 defects on the rows in 75 nm×75 nm $In_{0.53}Ga_{0.47}As(001)$–(4×2) surface. For the same size InAs(001)–(4×2) surface, there are only 23 D_1 defects on the rows. Therefore, there are at least 4 times more D_1 defects on the $In_{0.53}Ga_{0.47}As(001)$–(4×2) clean surface than on the InAs(001)–(4×2) clean surface since Fig. 1a represents one of the best $In_{0.53}Ga_{0.47}As(001)$–(4×2) surface that has been prepared while the InAs(001)–(4×2) in Fig. 1b is a typical surface.

Based on STM results, a RT $In_{0.53}Ga_{0.47}As(001)$–(4×2) structure model is proposed in Fig. 1e that shows undimerized In/Ga atoms in the top layer. The small scale filled state RT-STM images of the $In_{0.53}Ga_{0.47}As(001)$–(4×2) surface in Fig. 1c and d show more detailed information about the trough regions. For the RT $In_{0.53}Ga_{0.47}As(001)$, bright balls are imaged in the trough regions. The distance between the bright balls in the trough regions is 8.5 Å which is close to 2× the span of the $In_{0.53}Ga_{0.47}As(001)$ bulk unit cell (4.15 Å). However, the bright balls are not observed on InSb(001)–(4×2) and InAs(001)–(4×2) trough regions[18–23]. Conversely, the bright balls in the trough are observed for InAs growth on GaAs(001) surface by Xu et al. [34] and for indium-adsorbed onto the GaP(001) surface by Shimomura et al. [35], but the bright balls in the present study of group III rich $In_{0.53}Ga_{0.47}As$/InP(001) are smaller. In the present study of $In_{0.53}Ga_{0.47}As$/InP(001)–(4×2), the bright balls sometimes completely fill in the trough regions as shown in Fig. 1c, and sometimes only partially fill in the trough regions as shown in Fig. 1d. It is possible that these bright balls result from excess charges rather than atomic clusters, similar to what has been observed on the clean GaAs(001)–(4×2) surface [36,37]. However, further experiments are needed to better understand these results. Due to the lack of a regular, ordered existence of the bright balls on the surface and the fact that the bright balls appear to result from electrostatic rather than geometric origins, they will therefore not be considered for structural assignment on the $In_{0.53}Ga_{0.47}As(001)$–(4×2) surface.

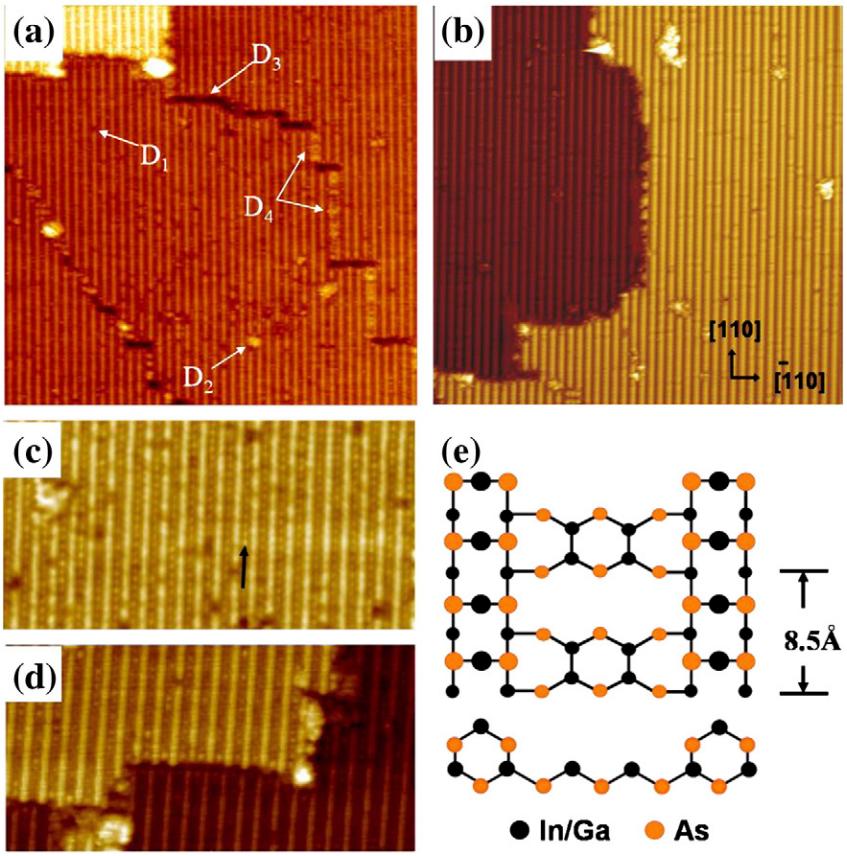

Fig. 1. STM of $In_{0.53}Ga_{0.47}As(001)$–$(4\times2)$ at 300 K. (a) Filled state (sample voltage −2 V, 75 nm×75 nm) RT-STM image of the group III rich $In_{0.53}Ga_{0.47}As(001)$–$(4\times2)$ surface. (b) Filled state (sample voltage −2 V, 75 nm×75 nm) RT-STM image of the group III rich InAs(001)–(4×2) surface. (c) Filled state (sample voltage −2.5 V, 38 nm×20 nm) RT-STM image of the group III rich $In_{0.53}Ga_{0.47}As(001)$–$(4\times2)$ surface with higher trough resolution where the bright balls completely fill in the trough region. (d) Same conditions as Fig. 1c except that the bright balls only partially fill in the trough region. (e) Ball-and-stick diagram of the group III rich $In_{0.53}Ga_{0.47}As(001)$–$(4\times2)$ at RT. There are at least four kinds of defects on the surface: D_1 as dark cuts on the row, D_2 as protrusion dots between the rows, D_3 domain boundaries as depression lines in the [−110] direction, and D_4 domain boundaries as protrusion lines in the [110] direction.

3.1.2. Low temperature 77 K $In_{0.53}$ $Ga_{0.47}As$ Surface

Fig. 2a shows a filled state STM image of group III rich $In_{0.53}Ga_{0.47}As(001)$ at low temperature (77 K). The LT-STM image pattern is distinctly different than the RT-STM image pattern, especially in rows along [110] direction (Fig. 2a and b). At 77 K, the space between the vertical rows is still 17 Å (4×) in the [−110] direction. However, the rows at LT are not continuous; instead, they are composed of separated bright blocks predominantly spaced 17 Å apart (4×) in the [110] direction. In the trough regions between the rows, no structure could be resolved. Based on STM images, a LT

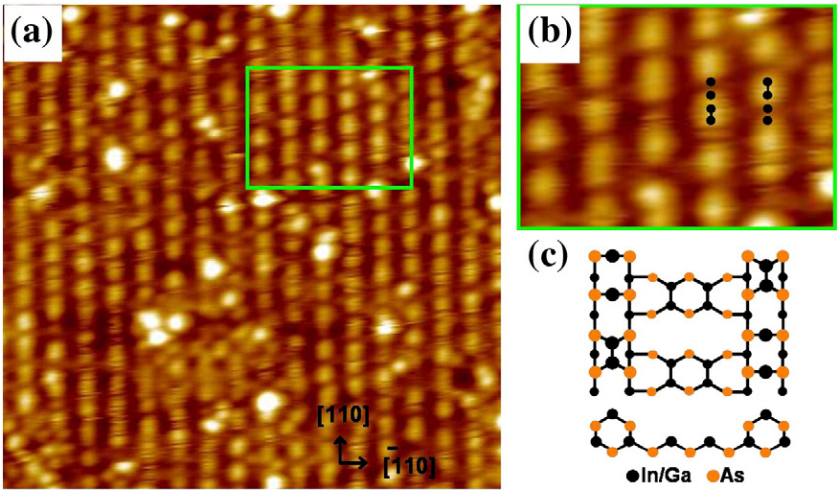

Fig. 2. STM of $In_{0.53}Ga_{0.47}As(001)$–$(4\times2)$ at 77 K. (a) A filled state (sample voltage −2 V, 30 nm×30 nm) LT-STM image of the group III rich $In_{0.53}Ga_{0.47}As(001)$ surface. (b) Expanded LT-STM image taken from the green box in Fig. 2a. (c) Ball-and-stick diagram of the group III rich $In_{0.53}Ga_{0.47}As(001)$ at LT. Note that the 8 black dots in Fig. 2b correspond to 8 In/Ga atoms on two In/Ga rows in Fig. 2c, 4 of them are dimerized and 4 of them are undimerized.

$In_{0.53}Ga_{0.47}As(001)$ structure model is proposed. Fig. 2c shows the ball-and-stick diagram of $In_{0.53}Ga_{0.47}As$ at LT. This structure consists of one In/Ga dimer and two undimerized In/Ga atoms per double (4×2) unit cell in the top layer [20]; note the detailed DFT results are explained in the calculations section. The positions of In/Ga dimer and undimerized In/Ga atoms in the row are assigned as black balls shown in Fig. 2b. The distribution analysis of dimer and spacing between dimers has been performed on InAs and InGaAs surfaces based on 77 K LT-STM data to determine most probable surface structures. The analysis shows that the most probable dimer and spacing between dimers for InGaAs and InAs are the same (8.4 Å). However, the distribution of dimer spacing is broader for InGaAs, and the second most common spacing is 12.6 Å. Several possible dimer and spacing structures are shown in Fig. 3e.

The phase transition between the RT (4×2) reconstruction and the LT reconstruction is reversible because the surface reconstructions are observed in both the transition from RT to LT and the transition from LT to RT directions. It is noted contaminants can be excluded from causing the LT reconstruction because (a) the RT surface structure can be recovered by heating the LT structure to RT; (b) the pressure in the STM chamber is below 1×10^{-10} Torr during cooling and LT imaging; (c) physisorbates rarely make ordered structures [20].

3.1.3. Electronic properties of $In_{0.53}Ga_{0.47}As$ surface

Scanning tunneling spectroscopy (STS) was used to determine the electronic properties of the surface. In STS, the tip is placed above the surface, and the tunneling current I(V), along with its first derivative dI/dV spectrum, is measured as a function of the tip-sample voltage. The positions of the band edges relative to 0 V (Fermi level) are used to determine the Fermi level position. Fig. 4a and b, shows STS spectra of the clean n-type and p-type $In_{0.53}Ga_{0.47}As(001)$–$(4\times2)$ surfaces at RT. These dI/dV curves were acquired at 15–20 different spots on the same surface for both n-type and p-type samples; afterwards, they are averaged to get STS results shown in Fig. 4. For each curve, one bandgap value and distance of Fermi level position relative to CBM or VBM are obtained. The experiments were repeated on 15 different samples using different tips to get the average value and standard deviation of Fermi level position relative to CBM or VBM. For clean n-type samples, the

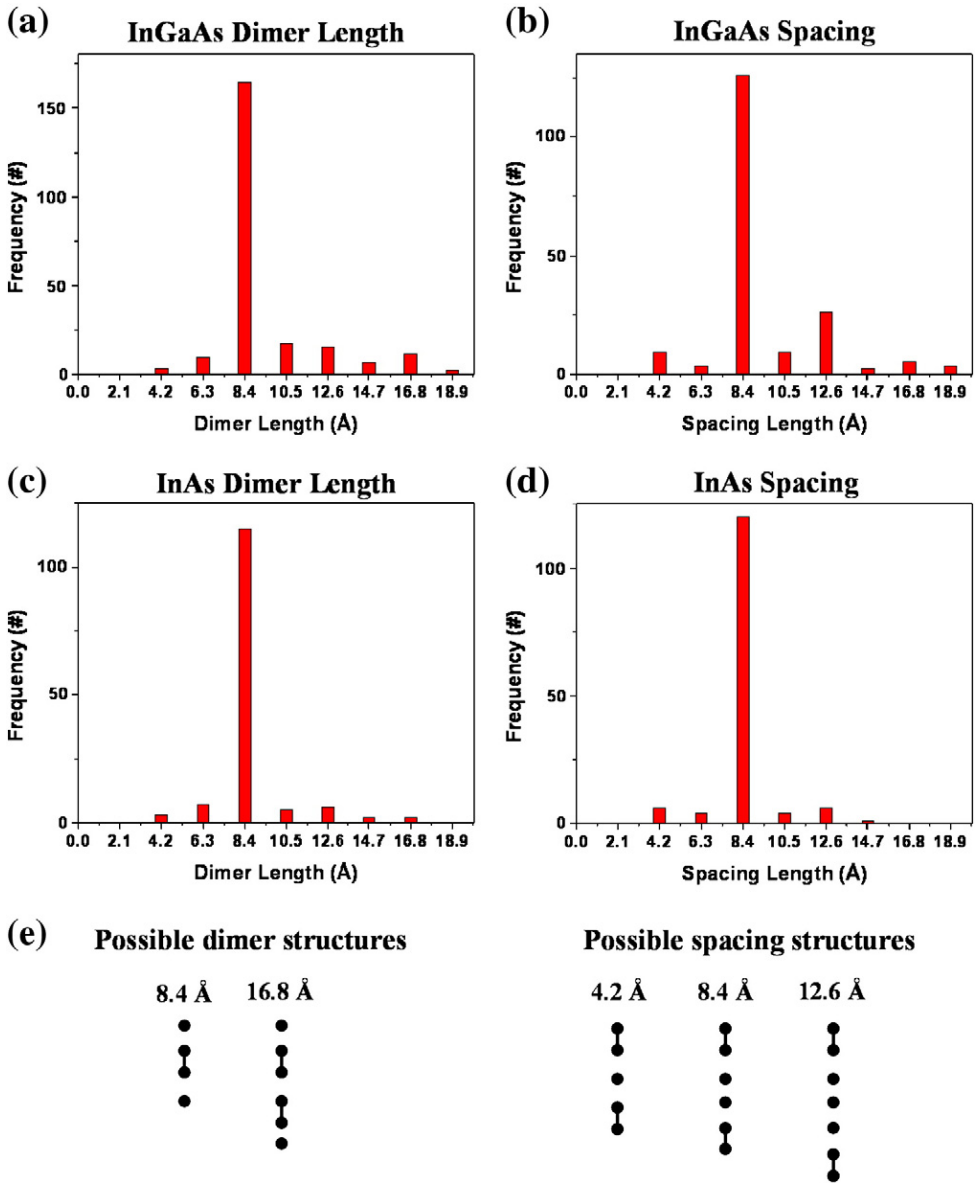

Fig. 3. The experimentally observed distribution of dimer lengths and spacings between dimers on InAs and InGaAs surfaces from 77 K LT-STM data. (a) InGaAs dimer length distribution. (b) InGaAs spacing distribution. (c) InAs dimer length distribution. (d) InAs spacing distribution. (e) Possible InAs and InGaAs dimer and spacing structures. The most probable surface structures for InAs and InGaAs are almost identical; however, InGaAs has broader dimer spacing distribution.

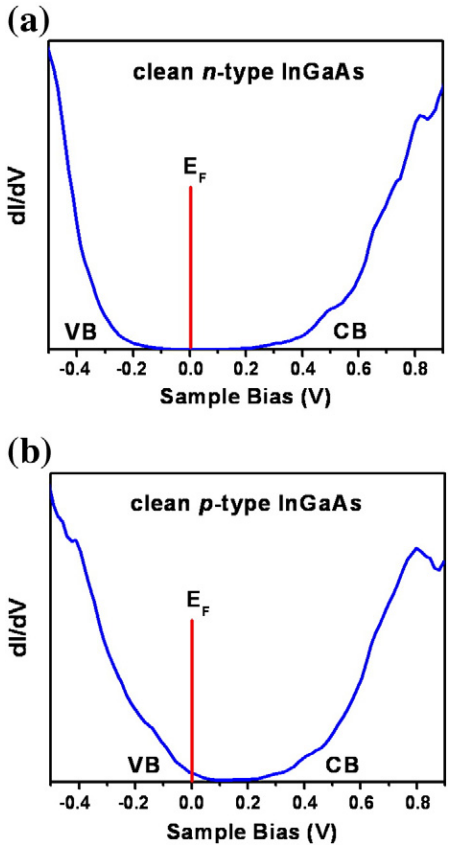

Fig. 4. Scanning tunneling spectroscopy for the following group III rich $In_{0.53}Ga_{0.47}As(001)$–$(4\times2)$ surfaces. (a) Clean n-type surface. (b) Clean p-type surface. For clean surfaces, the Fermi level (0 V) lies between the valence band (VB) and midgap for n-type, and near the VB for p-type. These results are based on statistical analysis of more 15 samples/STM tips.

Fermi level should reside near the conduction band (CB) for an unpinned dipole-free surface. However, the STS spectra on over 15 samples/STM tips shows that for n-type $In_{0.53}Ga_{0.47}As(001)$–$(4\times2)$ surface, the Fermi level resides between the midgap and the valence band (VB) (0.31 ± 0.18 eV close to VB). The Fermi level shift may be caused by surface band bending or by gap states; a surface dipole may exist due to differences in the number of filled and empty dangling bonds on the surface or from surface defects; a more detailed discussion can been found in Ref. [38]. For p-type $In_{0.53}Ga_{0.47}As(001)$–$(4\times2)$ surface, the Fermi level resides near the VB (0.26 ± 0.09 eV close to VB) which is typical for unpinned dipole-free surface but also consistent with a surface dipole or the pinning states near the VB.

3.2. Density functional theory results

In order to understand the difference in the surface reconstruction between 300 K and 77 K on $In_{0.53}Ga_{0.47}As(001)$, DFT calculations were performed on a series of structure models. In Fig. 5, five possible structures for the group III rich $In_{0.5}Ga_{0.5}As(001)$–(4×2) surface are shown along with their energy differences relative to the lowest total energy case (undimerized-buckled). Double unit cells are employed because of the large unit cell observed in the low temperature surface reconstruction. The criteria to distinguish all of these structures are whether the row is dimerized, undimerized or mixed, and whether the trough dimers are buckled or unbuckled. For example, the mixed-buckled structure consists of one In/Ga dimer and two undimerized In/Ga atoms in the row, and one buckled In/Ga dimer plus three unbuckled In/Ga dimers in the trough per double (4×2) unit cell. The undimerized-buckled structure consists of four undimerized In/Ga atoms in the row, and two buckled In/Ga dimers plus two unbuckled

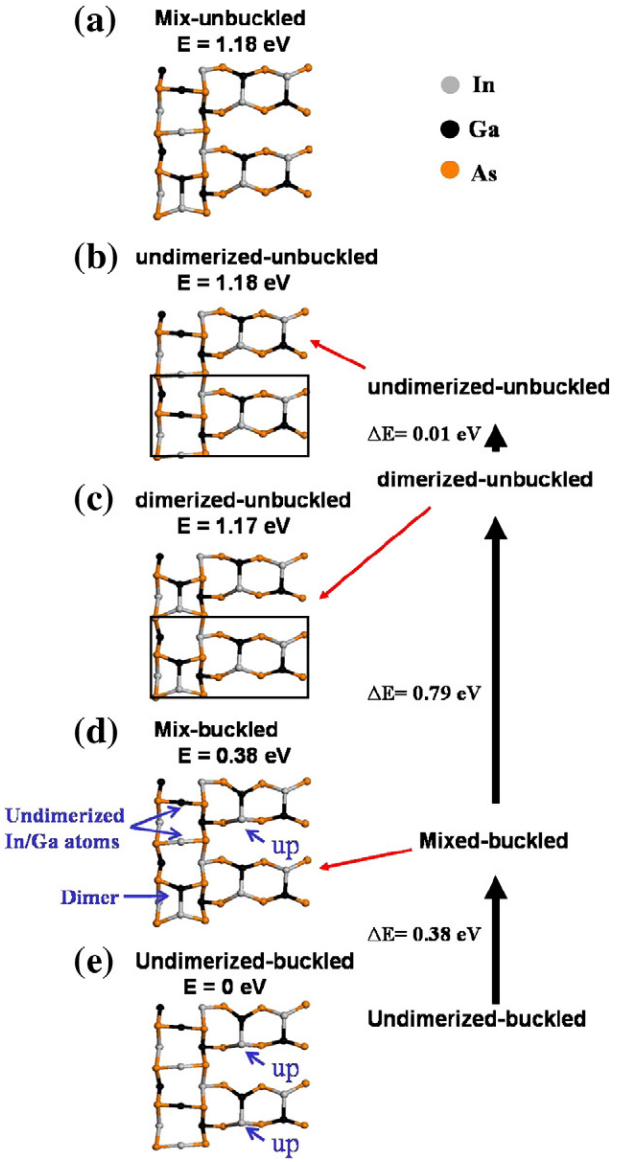

Fig. 5. Summary of possible surface structures for InGaAs(001) according to DFT calculations. Only the top atomic layers are shown for clarity of presentation. (a) Mixed-unbuckled structure. (b) Undimerized-unbuckled structure. (c) Dimerized-unbuckled structure. (d) Mixed-buckled structure. (e) Undimerized-buckled structure. Double unit cells are employed because of the large unit cell observed in the low temperature surface reconstruction. The dimerized-unbuckled and undimerized-unbuckled structures, and corresponding DFT calculation are based on a single unit cell which was extended into a double unit cell since a relaxed structure with unbuckled In/Ga dimers in the trough for a double unit cell could not be found. A single (4×2) unit cell is indicated in undimerized-unbuckled [Fig. 5b] and dimerized-unbuckled structures [Fig. 5c]. Other two InGaAs cases (mixed-buckled and undimerized-buckled structures) are based on a double unit cell. The energies shown in the figure is their energy differences relative to the lowest total energy case (undimerized-buckled). Buckled atoms in the upward position are highlighted with up symbol. Note Fig. 5a is not relaxed structure.

In/Ga dimers in the trough per double (4×2) unit cell. The main difference between the mixed-buckled structure and the undimerized-buckled structure is that for each double (4×2) unit cell, mixed-buckled structure has one row In/Ga dimer in the topmost layer and one buckled dimer in the trough, while undimerized-buckled structure has no row dimers and two buckled dimers in the trough. The relative energy differences in Fig. 5 are the total energy differences per double (4×2) unit cell. The dimerized-unbuckled and the undimerized-unbuckled structures, and their energy DFT calculations are based on a single unit cell, and, subsequently, extended into a double unit cell since there is no relaxed structure

found with unbuckled In/Ga dimers in the trough for a double unit cell calculation. The other two cases (mixed-buckled and undimerized-buckled structures) are based on a double unit cell. For mixed-unbuckled case, a relaxed stable structure was not obtained. The mixed-unbuckled energy shown in Fig. 5a is estimated based on the DFT calculated energies of dimerized-unbuckled and undimerized-unbuckled structures. From the relative energies in Fig. 5 of the dimerized-unbuckled and the undimerized-unbuckled structures, the dimerization energy for $In_{0.5}Ga_{0.5}As(001)$–(4×2) surface is estimated to be zero so the mixed-unbuckled energy is estimated to be degenerate with the dimerized-unbuckled and the undimerized unbuckled energies. Spin-polarization effects were also investigated, but spin-polarization did not affect the relative total energies.

3.2.1. Trough structure

According to the DFT calculations, structures with highly buckled trough dimers are predicted to be more stable than structures with only tilted trough dimers by at least 0.79 eV for InGaAs and 0.52 eV for InAs [20] per double unit cell. It is noted that the symmetry of the buckling in the trough is slightly different for the InGaAs(001)–(4×2) undimerized-buckled structure than the symmetry for the buckling in the trough for InAs(001)–(4×2) presented in Ref. [20] because of the propensity of In atoms to be in the up position. Two other highly buckled trough dimers structures with different buckling directions were also investigated, but buckling direction did not affect the total energies by more than 0.03–0.08 eV. The height difference between buckled and unbuckled dimers is around 1.2–1.3 Å. However, experimentally there is no strong evidence showing that the trough is buckled for InAs at both 300 K room temperature and 77 K low temperature [20]. For InAs, there are three experimental observations which strongly argue against the existence of extreme buckling in the trough: (a) STM image at 77 K of the trough clearly shows trough dimers without buckling; (b) the 77 K experimental structure clearly has mixed dimerized and undimerized In atoms on the row in contrast to the lowest energy structure calculated by DFT with buckled trough dimers; (c) the experimental reconstruction changes between 77 K and 300 K, but the DFT energy difference between mixed-buckled and undimerized-buckled InAs structures are more than 0.61 eV per double (4×2) unit cell which is inconsistent with the experimentally observed switch in reconstruction between 77 K and 300 K. Therefore, the extremely buckled structures were considered highly unlikely as possible structures for the InAs(001) surface. It was hypothesized that the DFT was not in agreement with the experiments for the trough structure because the limited cell size employed in DFT could not reproduce the strain in a real system with limited terrace size and surface defects. However, it is noted that even though buckled trough atoms were not observed at 77 K on InAs(0010)–(4×2), it is possible that the atoms in the trough are still fluctuating between buckled and unbuckled positions at 77 K.

For InGaAs case, there is no trough resolution at 300 K nor at 77 K but again three arguments apply: (a) The difference in height observed by STM between the row and trough is 1.2 to 1.5 Å at both 77 K and 300 K on both InAs(001)–(4×2) and InGaAs(001)–(4×2); this is consistent with the InAs(001)–(4×2) and InGaAs(001)–(4×2) having the same trough structures. This height does not match the difference in height between the relaxed row In/Ga atoms and unbuckled trough atoms in the DFT calculations (2.3 Å), but the same issue was observed with InAs(001)–(4×2) and is presumed to be due to the highly perturbed electronic structure of the trough atoms. (b) The 77 K experimental structure clearly has mixed dimers on the row in contrast to the lowest energy structure calculated by DFT with buckled trough dimers. (c) The experimental reconstruction changes between 77 K and 300 K, but the DFT energy difference between mixed-buckled and undimerized-buckled InGaAs structures are more than 0.38 eV per double (4×2) unit cell which is inconsistent with the experimentally observed switch in reconstruction between 77 K and 300 K. All the calculations shown in Fig. 5 assume that In/Ga atoms have equal distribution on the InGaAs surface. Since it is known that the InGaAs surface can be enriched in indium due to surface segregation [39], the DFT calculations were also run with only In atoms in the topmost layer. The energy differences between these cases were similar to the non-In enriched surface. When the surface layer consists of only indium atoms, there is still buckling in the trough consistent with the buckling not being an artifact of the choice of a regular polymorph for InGaAs. The difference between experiment and theory for unbuckled and buckled is probably due to the inability of the small slab to capture the proper strain relaxation of the experimentally observed surface which has terraces sizes well over 10–100× larger than the double unit cells employed in these calculations.

3.2.2. Row structure

For the other three structures: dimerized-unbuckled, undimerized-unbuckled and mixed-unbuckled, since the trough structures remain same, the main difference lies on the row structure. For unbuckled InGaAs(001) surface, the dimerization energy is about 0 eV. All three unbuckled InGaAs(001) reconstructions are energetically degenerate.

A DFT molecular dynamics (MD) study was performed to determine if the surface row fluctuates between the dimerized structure (mixed-unbuckled) and the undimerized structure (undimerized-unbuckled) at elevated temperature. In these calculations, the trough dimers (8 In/Ga atoms) and 12 adjacent to them As atoms were fixed in the z direction in the nearly flat positions of the dimerized-unbuckled relaxed structure to provide a realistic simulation of the experimentally observed structures; all other surface and subsurface atoms were free to move except the bottom three layers which were always fixed in their bulk-like positions. The InGaAs sample was DFT annealed at 900 K for 1000 fs with a 1.0 fs time steps. The elevated temperature was employed instead of 300 K to reduce the number of time steps required to simulate dimer breaking and formation. The results were checked by doing simulations at a second elevated temperature (1200 K). Fig. 6 shows the row structures of InGaAs clean surface annealed at 900 K at different annealing times (fs). The 125 fs and 126 fs snapshots are the transition structures before and after row dimer breaking. The 324 fs and 325 fs snapshots are the transition structures before and after row dimer formation. The 779 fs and 780 fs snapshots are the transition structures before and after row dimer re-breaking. These results clearly show that surface row dimers can spontaneously break their dimer bonds and switch back to form dimer bonds between three unbuckled structures since the total energy difference is so small. In a simple Arrhenius model, since the formation/breaking time is 260 fs at 900 K, the formation/breaking time should be about 2 ps at 300 K. The estimated 300 K fluctuation time is faster than the STM scanning time (around 100 ms) consistent with a 300 K surface showing an undimerized-unbuckled surface structure due to a thermal superposition of dimerized-unbuckled, undimerized-unbuckled and mixed-unbuckled structures since undimerized row structures have higher symmetry.

A detailed analysis of the annealing calculation shows the mechanism of rapid dimer formation and breaking. In the initial structure (0 fs), the row is mixed with one In/Ga dimer and two undimerized In/Ga atoms. The bond angles between edge As atoms and row In/Ga atoms are different for the undimerized and dimerized structures. For the undimerized structure, the bond angles are between 166° and 178°, consistent with sp hybridization. For dimerized structure, the bond angles are between 138° and 143° consistent with a strained sp^2 hybridization since these bond angles are slightly larger than the ideal 120° for sp^2 hybridized system. At 125 fs, As atoms 5, 6 and their neighboring row Ga atom move in the positive x direction, and As atoms 7, 8 and their neighboring In atom move in the negative x direction. The bond length between the

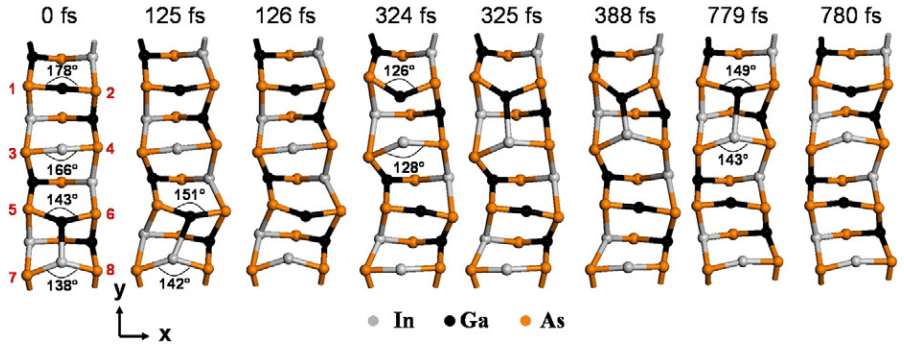

Fig. 6. DFT molecular dynamics (MD) model of the row structures of InGaAs clean surface annealed at 900 K at different annealing times in femtoseconds (fs). Bond angles for atomic positions are calculated to assist in determining the mechanisms of row dimers formation and breaking. The normal to the paper is the z direction.

dimerized In and Ga atoms is expanded from 2.79 Å (0 fs, dimerized In/Ga atoms) to 3.16 Å (125 fs). This twist bending mode makes this row dimer break.

At 324 fs, As atoms 1, 2, 3, 4 and the undimerized neighboring row In/Ga atoms all are moving in the negative x direction. At 324 fs, these In/Ga atoms are also moving upwards in the z direction increasing their bond angles with the row edge As atoms to 126°–128° thereby forming a sp^2 geometry which allows row dimer formation. Simultaneously, the bond length between these Ga and In atoms becomes shorter, from 4.20 Å (0 fs, undimerized In/Ga atoms) to 3.10 Å (324 fs). The initial row bond formed at 324 fs is not completely relaxed; at 388 fs, the In/Ga atoms are closer (2.48 Å). After 388 fs, the In/Ga atoms bond length becomes larger and the upper row dimer start to break. At 779 fs, the upper row In/Ga dimer bond length is 3.17 Å, and these In/Ga are moving back close to the initial structure (0 fs, undimerized In/Ga atoms) in the z direction causing the bond angle to increase and thereby breaking the dimer at 780 fs.

In summary, three ways to form or break the row dimers were observed in the DFT-MD simulations: (a) as shown in the 125 fs diagram, a large twist and bend greatly elongates an In/Ga dimer bond thereby breaking a dimer bond; (b) as shown in the 324 fs diagram, a In/Ga upwards z direction motion decreases the bond angles from sp to sp^2 thereby forming a dimer bond; (c) as shown in the 779 fs diagram, In/Ga downwards z direction motion increases the bond angles from sp^2 to sp thereby breaking a dimer bond.

77 K STM experimental results strongly suggest that the most probable row structure for InGaAs is mixed row structure, which consists of one In/Ga dimer and two undimerized In/Ga atoms in the row per double unit cell. However, there is another probable row structure for InGaAs surface (12.6 Å) shown in Fig. 3. This is similar to Ge(001)–(2×1) cases at RT and LT [36]. At RT, In/Ga atoms in the top layer fluctuate between the dimerized structure and the undimerized structure. At LT, the surface atoms are frozen. The same DFT-MD study was performed on InAs(001)–(4×2) using the identical DFT parameters employed for InGaAs(001)–(4×2). Again at 900 K, starting with an initial mixed row structure and flat trough dimers, row dimer breaking and formation was observed on within the 1000 fs simulation time. The mechanisms of row dimer formation and breaking were almost identical, the extreme motion of row edge As atoms increasing the In–In dimer bond length weakening the In–In bond, z motion induced changes in bond angles, and extreme dimer bond lengthening. These results are consistent with the 300 K InAs(001)–(4×2) structure also being a thermal superposition (see supplemental materials).

3.2.3. Density of states

The density of states (DOS) of dimerized-unbuckled, mixed-buckled, and undimerized-buckled structures have been studied to identify the source of the Fermi level pinning. DOS was calculated and shown in the bandgap region. Both mixed and undimerized-buckled structures contain row In/Ga atoms making only two bonds with row edge As atoms; these atoms are sp hybridized in contrast to nearly all other III–V surface reconstructions except InAs(001)–(4×2) [20]. The atoms are considered sp hybridized due to their coordination to two atoms while having close to 180° bond angles. It is surprising to find stable sp hybridized atoms on a group III rich surface since all other known surface reconstructions have only sp^2 and sp^3 hybridized atoms on the surfaces. These sp hybridized In/Ga atoms may have dangling bonds which pin the Fermi level. Fig. 7c shows the DOS results of the clean undimerized-buckled $In_{0.5}Ga_{0.5}As(001)$ surface. There is a reasonable bandgap containing no states for undimerized-buckled structure. This shows that the sp hybridized atoms do not pin the Fermi level.

The trough dimers are a likely source of the Fermi level pinning since they are in a strained atomic geometry. Each of the tricoordinated In/Ga atoms in the trough has an empty dangling bond so the relaxed geometry would be triangular planar sp^2 bonding; instead, in the unbuckled geometry from the DFT model, the trough In/Ga atoms are in a tetrahedral sp^3 geometry. Buckling of the trough In/Ga dimer allows the dimer atom in the down position to have a more sp^2 bonding geometry while placing the dimer atom in the upward position to be in a more sp^3 bonding geometry; this would be unstrained if there was charge transfer to the atoms in the upward position to fill their dangling bonds. As shown in Fig. 7, for unbuckled and mixed-buckled structures, there is no bandgap consistent with the strained unbuckled trough dimers or the row dimers in these reconstructions pinning the Fermi level.

To identify whether the strained unbuckled trough dimers or the row dimers, or both of them pin the Fermi level, the band-decomposed electron charge densities for the mixed-buckled and the undimerized-buckled structures are calculated and plotted in Fig. 8. The bandgap states are visualized by calculating and summing band-decomposed charge density between −0.25 eV and 0.25 eV for the pinned mixed-buckled structure; the valence band edge states are visualized by calculating and summing the band-decomposed charge density between −0.5 eV and 0 eV (with Fermi level $E_f = 0$ eV) for the unpinned undimerized-buckled structure; the conduction band edge states are visualized by calculating and summing the band-decomposed charge density between 0 eV and +0.5 eV for the unpinned undimerized-buckled structure.

The spatial distribution of bandgap states shows that the mixed-buckled structure has pinning states localized at the strained unbuckled trough dimers and no pinning states on the row atoms, as shown in Fig. 8a. This result is consistent with surface pinning of group III rich $In_{0.5}Ga_{0.5}As(001)$–(4×2) being caused by the strained unbuckled trough dimers, and not by the row atoms. For the undimerized-buckled structure, the buckling of the trough dimers relieves the stress and unpins the surface. The filled valence band edge state distribution for undimerized-buckled structure is localized on

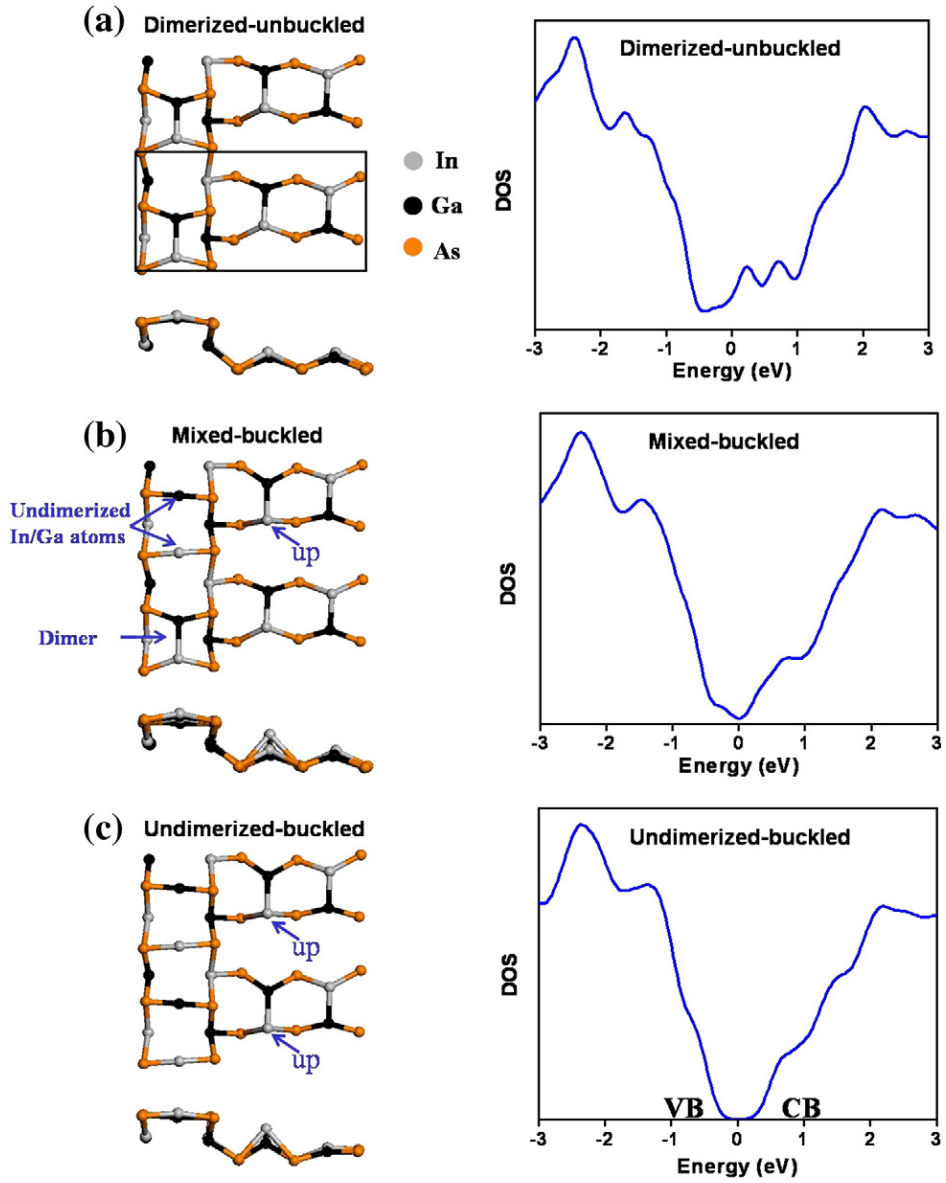

Fig. 7. DFT relaxed atomic structures and density of states (DOS) curves for group III rich $In_{0.5}Ga_{0.5}As(001)$ reconstructions. The dimerized-unbuckled and mixed-buckled structures have no bandgap, and the surfaces are pinned. The undimerized-buckled structure has a bandgap, and the surface is unpinned.

the buckled In/Ga atoms in the trough and while the empty conduction band edge states are localized on the undimerized In/Ga atoms in the row.

A top view of the undimerized-buckled band edge filled states from −0.5 eV to 0 eV and empty states from 0 eV to +0.5 eV shows there is only empty orbital overlap between the sp In/Ga atoms consistent with the row sp In/Ga atoms forming π bonding with the row edge As atoms instead of forming partially filled dangling bonds.

Since the 300 K data is expected to be a superposition of isomers of the three unbuckled structures, DFT predicts a pinned Fermi level for the clean $In_{0.5}Ga_{0.5}As(001)$ surface consistent with the data. To better understand the mechanism of the pinning by the unbuckled trough dimers, the Bader charges on all the surface atoms were calculated [40–42]. The Bader charges of atoms are obtained by spatial decomposition of 3D field of converged electron density to regions centered at particular atoms and subsequent charge density integration within these regions. The 3D charge density field is decomposed to atomic regions by performing a gradient analysis and finding zero-flux surfaces around atoms. The Bader charge approach provides much more meaningful and physically correct charge calculation for plane-wave DFT calculations than charge density integration within spherical regions of empirical atomic radii. Note, that a Bader charge having a positive value indicates number of valence electrons associated with a particular atom. In the present simulations, positive Bader charge differences indicate increasing of the electron charges associated with the atoms, which makes the atoms more negatively charged. The relative charge differences are calculated from Bader charge differences between surface atoms and bulk atoms. For example, the tricoordinated row edge As atoms lose electrons compared to bulk As atoms so they are shown with negative changes in Bader charge in Fig. 8.

In Fig. 8, the results show all the surface atoms have close to bulk-like charge for both mixed-buckled and undimerized-buckled structures, and the largest charge transfer is only ~0.3 electrons for any of the surface atoms. Comparing Bader charges between mixed-buckled (pinned structure) and undimerized-buckled (unpinned structure), in the unpinned undimerized-buckled structure, two row In/Ga atoms in the lower half of the row lose a total of 0.19 electrons, the four As atoms at the edge of row lose a total of 0.24 electrons, and the In/Ga dimer in the lower left of the trough gains 0.2 electrons. The breaking of the row

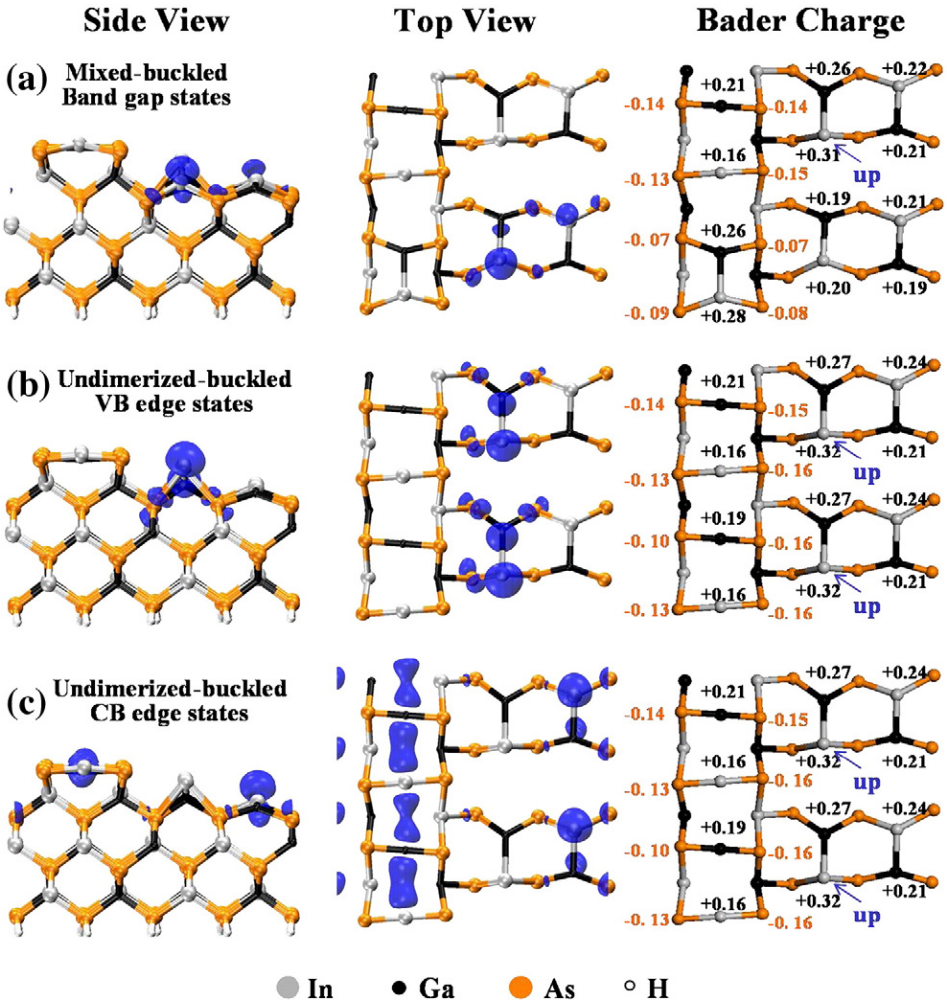

Fig. 8. The band-decomposed electron charge densities and Bader charge differences relative to in-bulk atoms of group III rich $In_{0.5}Ga_{0.5}As(001)$ for the mixed-buckled and undimerized-buckled. (a) The mixed-buckled structure with the charge density summed between −0.25 eV and +0.25 eV; the contour spacing is $5\times10^{-3}eÅ^{-3}$. (b) The undimerized-buckled structure with the band edge filled states charge density summed between −0.5 eV and 0 eV (Fermi level $E_f=0$ eV); the contour spacing is $1\times10^{-2}eÅ^{-3}$. (c) The undimerized-buckled for band edge empty states with the charge density summed between 0 eV and +0.5 eV; the contour spacing is $2\times10^{-3}eÅ^{-3}$. The charge density is in blue. The buckled atoms in the upward position are highlighted with up symbol in the third column. For the top view and the Bader charge view, only the top three atomic layers are shown. For the Bader charges, the relative charge differences are shown. The relative charge differences are calculated from differences between surface atoms and bulk atoms.

dimers bonds induces a buckling of one of the trough dimers, and the buckling causes a charge transfer of about 0.2 electrons to the trough dimer which partially fills the dangling bond on the buckled trough atoms partially relieving the strain. In essence, the unpinning is accompanied by a small charge transfer from the rows to the buckled trough dimer stabilizing the atom in the sp^3 buckled up position. This is consistent with the buckled trough dimers being unpinned and the unbuckled trough dimers being pinned as shown by the bandgap states in Fig. 7(a). Although the DFT model is consistent with the STS data, it is noted that the high density of surface defects may affect the experimental electronic properties of $In_{0.5}Ga_{0.5}As(001)$–(4×2).

4. Conclusions

STM images of the decapped group III rich $In_{0.53}Ga_{0.47}As(001)$ surface reconstruction have been obtained at both 300 K and 77 K. Empirically, the STM results are consistent with different surface reconstructions. At 300 K, STM images show that the $In_{0.53}Ga_{0.47}As$ (001) surface reconstruction is comprised of undimerized In/Ga atoms in the top layer. Conversely, 77 K STM images show that the $In_{0.53}Ga_{0.47}As(001)$ surface reconstruction is primarily comprised of one In/Ga dimer and two undimerized In/Ga atoms in the top layer in a double (4×2) unit cell. STS results show that for clean 300 K surfaces, the Fermi level resides between the valence band (VB) and midgap for n-type, and near the VB for p-type consistent with the RT surface being either pinned or having a large surface dipole. DFT molecular dynamics (MD) simulations show that the 300 K structure is not a unique structure distinct from the 77 K structure but instead the experimentally observed 300 K structure is consistent with a thermal superposition of three structures including the 77 K structure. DFT-MD show the row dimer formation and breaking is facilitated by the very large motions of tricoodinated row edge As atoms and z motion of In/Ga row atoms induced changes in As–In/Ga–As bond angles at elevated temperature. DFT calculations of the band-decomposed charge density indicate that the strained unbuckled trough dimers being responsible for the surface pinning.

Acknowledgments

The authors would like to thank M. Passlack and T. Grassman for valuable discussions, and E.A. Carter for a helpful discussion concerning density functional theory. J. Shen acknowledges PhD Foundation Fellowship from the Intel Corporation. This work was supported by SRC-NCRC-1437.003, and the FCRP-MSD-887.011 and NSF-DMR.

Appendix 1. Supplementary data

Supplementary data associated with this article can be found, in the online version, at doi:10.1016/j.susc.2010.07.001.

References

[1] M.J. Hale, S.I. Yi, J.Z. Sexton, A.C. Kummel, M. Passlack, The Journal of Chemical Physics 119 (2003) 6719.
[2] A. Chakrabarti, P. Kratzer, M. Scheffler, Physical Review B 74 (2006) 11.
[3] J. Mirecki Millunchick, A. Riposan, B.J. Dall, C. Pearson, B.G. Orr, Surface Science 550 (2004) 1.
[4] P.A. Bone, J.M. Ripalda, G.R. Bell, T.S. Jones, Surface Science 600 (2006) 973.
[5] P. Kruse, J.G. McLean, A.C. Kummel, The Journal of Chemical Physics 113 (2000) 9217.
[6] P. Kruse, J.G. McLean, A.C. Kummel, The Journal of Chemical Physics 113 (2000) 9224.
[7] S.I. Yi, P. Kruse, M. Hale, A.C. Kummel, The Journal of Chemical Physics 114 (2001) 3215.
[8] D.L. Winn, M.J. Hale, T.J. Grassman, J.Z. Sexton, A.C. Kummel, The Journal of Chemical Physics 127 (2007) 134705.
[9] J.B. Clemens, S.R. Bishop, D.L. Feldwinn, R. Droopad, A.C. Kummel, Surface Science 603 (2009) 2230.
[10] G. Kresse, J. Furthmuller, Physical Review B 54 (1996) 11169.
[11] G. Kresse, J. Furthmuller, Computational Materials Science 6 (1996) 15.
[12] P.E. Blochl, Physical Review B 50 (1994) 17953.
[13] G. Kresse, D. Joubert, Physical Review B 59 (1999) 1758.
[14] J.P. Perdew, K. Burke, M. Ernzerhof, Physical Review Letters 77 (1996) 3865.
[15] J.P. Perdew, K. Burke, M. Ernzerhof, Physical Review Letters 78 (1997) 1396.
[16] K. Shiraishi, Journal of the Physical Society of Japan 59 (1990) 3455.
[17] J. Neugebauer, M. Scheffler, Physical Review B 46 (1992) 16067.
[18] M.O. Schweitzer, F.M. Leibsle, T.S. Jones, C.F. McConville, N.V. Richardson, Surface Science 280 (1993) 63.
[19] C. Kendrick, G. LeLay, A. Kahn, Physical Review B 54 (1996) 17877.
[20] D.L. Feldwinn, J.B. Clemens, J. Shen, S.R. Bishop, T.J. Grassman, A.C. Kummel, R. Droopad, M. Passlack, Surface Science 603 (2009) 3321.
[21] A.A. Davis, R.G. Jones, G. Falkenberg, L. Seehofer, R.L. Johnson, C.F. McConville, Applied Physics Letters 75 (1999) 1938.
[22] P. De Padova, P. Perfetti, C. Quaresima, C. Richter, O. Heckmann, M. Zerrouki, R.L. Johnson, K. Hricovini, Surface Science 532 (2003) 837.
[23] G. Goryl, O. Boelling, S. Godlewski, J.J. Kolodziej, B. Such, M. Szymonski, Surface Science 601 (2007) 3605.
[24] D.K. Biegelsen, R.D. Bringans, J.E. Northrup, L.E. Swartz, Physical Review B 41 (1990) 5701.
[25] S.L. Skala, J.S. Hubacek, J.R. Tucker, J.W. Lyding, S.T. Chou, K.Y. Cheng, Physical Review B 48 (1993) 9138.
[26] Q.K. Xue, T. Hashizume, J.M. Zhou, T. Sakata, T. Ohno, T. Sakurai, Physical Review Letters 74 (1995) 3177.
[27] P. Moriarty, P.H. Benton, Y.R. Ma, A.W. Dunn, M. Henini, D.A. Woolf, Journal of Vacuum Science and Technology B 14 (1996) 943.
[28] I. Chizhov, G. Lee, R.F. Willis, D. Lubyshev, D.L. Miller, Surface Science 419 (1998) 1.
[29] S.H. Lee, W. Moritz, M. Scheffler, Physical Review Letters 85 (2000) 3890.
[30] J.E. Northrup, S. Froyen, Physical Review Letters 71 (1993) 2276.
[31] J.E. Northrup, S. Froyen, Physical Review B 50 (1994) 2015.
[32] D.J. Chadi, Journal of Vacuum Science and Technology A 5 (1987) 834.
[33] G.-X. Qian, R.M. Martin, D.J. Chadi, Physical Review B 38 (1988) 7649.
[34] Q.K. Xue, Y. Hasegawa, T. Ogino, H. Kiyama, T. Sakurai, Journal of Vacuum Science and Technology B 15 (1997) 1270.
[35] M. Shimomura, D. Ichikawa, G.P. Srivastava, K.Z. Liu, Y. Fukuda, Physical Review B 78 (2008) 5.
[36] P. Kruse, J.G. McLean, A.C. Kummel, The Journal of Chemical Physics 113 (2000) 2060.
[37] J.J. Kolodziej, B. Such, M. Szymonski, Physical Review B 71 (2005) 7.
[38] J. Shen, E.A. Chagarov, D.L. Feldwinn, W. Melitz, N.M. Santagata, A.C. Kummel, R. Droopad, M. Passlack, submitted to Journal of Chemical Physics (2010).
[39] J.M. Moison, C. Guille, F. Houzay, F. Barthe, M. Vanrompay, Physical Review B 40 (1989) 6149.
[40] G. Henkelman, A. Arnaldsson, H. Jonsson, Computational Materials Science 36 (2006) 354.
[41] E. Sanville, S.D. Kenny, R. Smith, G. Henkelman, Journal of Computational Chemistry 28 (2007) 899.
[42] W. Tang, E. Sanville, G. Henkelman, Journal of Physics: Condensed Matter 21 (2009) 7.